J Electr Eng Technol.2018; 13(4): 1586-1595
http://doi.org/10.5370/JEET.2018.13.4.1586

ISSN(Print) 1975-0102
ISSN(Online) 2093-7423

Magnetic Field Calculation and Multi-objective Optimization of Axial Flux Permanent Magnet Generator with Coreless Stator Windings

Zhu Jun†, Li Shaolong*, Song Dandan*, Han Qiaoli and Li guanghua***

Abstract – For the problem that the complexity of 3-D modeling and multi parameter optimization, as well as the uncertainty of the winding factor of axial flux permanent magnet generator with coreless windings. The complex 3-D model was simplified into 2-D analytic model, and an analytical formula for the winding factor that adapting different coreless stator winding is proposed in this paper. The analytical solution for air-gap magnetic fields, no-load back EMF, electromagnetic torque, and efficiency are calculated by using this method. The multiple objective and multivariable optimization of the maximum fundamental and the minimum harmonic content of back EMF are performed by using response surface methodology. The proposed optimum design method was applied to make a generator. The generator was tested and the calculated results are compared with the proposed method, which show good agreements.

Keywords: Axial flux, Coreless winding factor, 2-D analytical model, Response surface methodology, Finite element method.

1. Introduction

Axial flux permanent magnet synchronous generator (AFPMSG) has more advantages than traditional motor. It has the advantages of small axial dimension, compact structure, high efficiency and large power density. The double external rotor and coreless internal stator structure not only reduces the weight of the motor and eliminate the cogging torque and the core loss which has a small starting torque, high efficiency and is very suitable for small stand-alone wind power generation system[1-5].

AFPMSG adopts non overlapping winding, which has more advantages than distributed winding, such as short end length of winding, less copper consumption and less heating loss [6]. The disadvantage is that the winding factor of the non overlapping winding is relatively low, the output torque is small, the spatial layout is diverse, which could influence the magnetic density distribution of motor. Higher winding factor and better output torque can be obtained by using non overlapping concentrated windings when the number of poles is large [7]. The more the number of poles is, the lower the speed. So the AFPMSG multi pole structures are suitable for the areas with small wind speed especially and utilizing wind resources effectively.

The coreless main magnetic field of AFPMSG is a three-dimensional structure. The most accurate design method is the 3-D finite element method. However, the 3-D finite element modeling is a multi-objective and multi variable process. The optimization process is complex, time-consuming and higher requirements to the performance of computer. On the other hand, the coreless stator is not limited by the groove shape, and the winding structure will affect the winding factor and the gap density distribution.

The common analysis method of magnetic field is that changing the magnetic field of a motor into a quasi static electromagnetic field, and only analyze the magnetic field produced by the excitation of a permanent magnet. The analytical formula of air gap flux density can be obtained by solving the Maxell equation. Then the back EMF and electromagnetic torque are analyzed by winding flux linkage [8,9]. But this method is only suitable for the fixed winding structure, and it is not suitable for the structure of coreless stator windings. For the slot motor with an iron core, the coil is placed in the slot, and the winding layout is limited by the slot type. The winding factor is determined by the pitch factor and is easy to be calculated. The calculation formula were derived from the stator winding factor groove structure [10, 11], but the calculation of coreless winding factor for different winding structure is more complex without groove limit. In the same coil, the back EMF of the wire is different in different positions. Therefore, when calculating the winding factor, in addition to the pitch factor, the winding factor should also be considered in the single span of the coil. The width of the coil is only 1/3 of the coil's span when the fundamental wave is considered [12]. But the width of the coil edge under harmonic condition is not taken into full consideration. The winding factor of coreless linear motor is calculated by reference [13]. This method needs to consider the

† Corresponding Author: School of Electrical Engineering and Automation, Henan Polytechnic University, Jiaozuo, 454000, China (zhujunnd@163.com)
* School of Electrical Engineering and Automation, Henan Polytechnic University, China
** School of Energy and Transportation Engineering, Inner Mongolia Agricultural University, China
Received: October 18, 2017; Accepted: February 26, 2018

complicated calculation process of multivariable. Three different concentrated winding factors structures were compared [14]. But it did not analyze the influence of the change of the width and thickness on the overall performance of the motor.

In this paper, the 3-D model of AFPMSG is simplified into 2-D linear model. An analytical formula for the winding factor that adapt to different coreless stator is proposed. The response surface method is applied to optimize the multi-objective and multivariable generator in order to achieve the maximum fundamental wave and the minimum harmonic content of the back EFM. In order to verify the result of the optimal design method, a prototype generator is designed according to this method. The results obtained by the analytical method and the response surface optimization method are compared with the 3-D finite element method and the measured values of the prototype. The maximum error is within 7%, and the correctness of the method is verified.

2. Model and Magnetic Field Solutions

The coreless stator of AFPMSG structure is shown in Fig. 1. Its 3-D model looks like a disc-type machine. The coreless stator winding is irrigated and fixed by epoxy resin. The permanent magnets are magnetized along the axial direction. The two adjacent permanent magnets of the same rotor disc have opposite directions of magnetization, and the two opposite permanent magnets of the different rotor disks have the same direction of magnetization.

If we use the 3-D model of the whole motor to do the finite element simulation directly, the main flux is in z axis direction, the solution area is large, the mesh that needs to be divided is more, the computation speed is very slow, sometimes the computer memory can not be calculated. Therefore, when the finite element simulation is carried out, a reasonale selection of the solution area is needed to reduce the amount of calculation.

It can be seen from the distribution of coreless AFPMSG magnetic field, the magnetic field along the circumferential direction is symmetrical, and one electrical period is two pole distance. Its magnetic field is symmetrical about the center of the axis of the generator. Therefore, a pair of magnetic poles can be selected to establish the 2-D model, and the main magnetic field of the *z* axis in the 3-D model

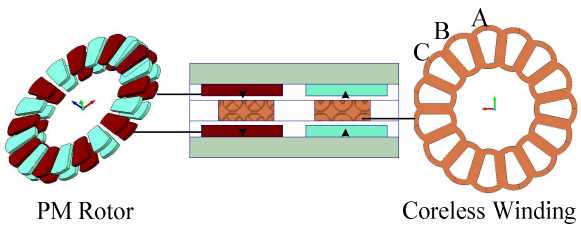

Fig. 1. AFPMSG with coreless stator windings

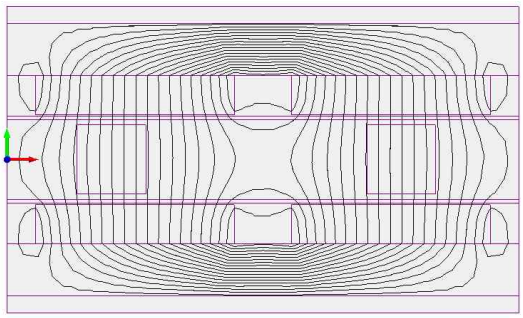

(a)

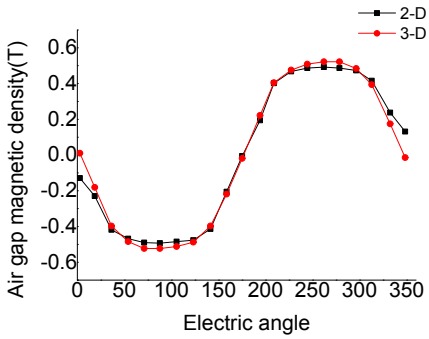

(b)

Fig. 2. (a) 2-D FEA model, (b) comparison of analytical results with 3-D

is converted into the *y* axis direction magnetic field of the 2-Dmodel to analyze the magnetic field. The 2-D magnetic field distribution and finite element results are as shown in Fig. 2(a) and Fig. 2(b).

2.1 2-D analytical model

The internal magnetic circuit in the axial flux permanent magnet synchronous generator is distributed along the circumferential direction in the back iron, and distributed along the axial direction in the permanent magnet and the air gap. The stator coreless magnetic circuit is not saturated. In order to simplify the 3-D model, ignoring the magnetic field changing in the direction of the *z* axis of the permanent magnet, using a negligible thickness cylindrical surface along the axial direction to intercept the generator at the average radius. The result cross section is the generator's 2-D model [15], as shown in Fig. 3(a). The origin is the midpoint of the boundary between the permanent magnet and the back iron. The *x* axis represents the circumferential distance, and the *y* axis represents the axial distance.

2.2 2-D magnetic field calculation

The air gap of the coreless axial flux generator is relatively large, and the influence of the generator current is not considered in the no-load calculation. The magnetic field is only generated by the permanent magnet excitation,

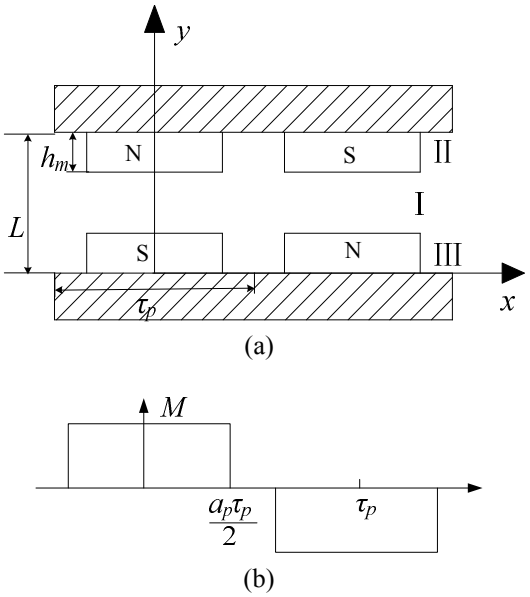

Fig. 3. 2-D Magnetic field analysis model, (a) Layered model (b) PM magnetization

it is assumed that :

1) all regions are extended to infinitely in the *x* direction, and the permanent magnet is magnetized uniformly in the *y* direction;

2) the magnetic density of rotor back is not saturated, and its permeability is infinite;

3) the permeability of the permanent magnet is the same as that of the air permeability in all directions.

The magnetic field produced by the permanent magnet is divided into three regions, the middle air gap region I, the air part between the upper rotor permanent magnet and the permanent magnet is region II, and the under rotor permanent magnet region III [16-20].

$$\begin{cases} \dfrac{\partial^2 A_{\mathrm{I}}(x,y)}{\partial x^2}+\dfrac{\partial^2 A_{\mathrm{I}}(x,y)}{\partial y^2}=0 \\ \dfrac{\partial^2 A_{\mathrm{II}}(x,y)}{\partial x^2}+\dfrac{\partial^2 A_{\mathrm{II}}(x,y)}{\partial y^2}=-\mu J_{\mathrm{M}} \end{cases} \tag{1}$$

The permanent magnet is axially parallel magnetized. There is only *y* directional component in the 2-D model. Its magnetization is shown in Fig. 3(b). The magnetization intensity of B_r in the *y* direction of a permanent magnet with M_y can be expressed by Fourier series:

$$M_y=\sum_{n=1,3,5...}^{\infty} M_n\cos\frac{n\pi x}{\tau_p} \tag{2}$$

where *n* is the harmonic number:

$$M_n=\frac{4B_r}{n\pi\mu_0}\sin\frac{n\pi\alpha_p}{2} \tag{3}$$

B_r is the residual magnetic flux density of permanent magnetic material, *x* is the coordinate along the armature surface, *n* is the harmonic number, τ_p is polar pitch, μ_0 is the permeability of vacuum. The air gap flux density in the *y* direction is obtained by solving the Maxell equation:

$$B_y(x,y)=\frac{8B_r}{\pi}\sum_{n=1,3,5...}^{\infty}\frac{B_n}{\Lambda}\cosh\frac{n\pi(L/2-y)}{\tau_p}e^{\frac{n\pi L}{2\tau_p}}\cos\left(\frac{n\pi}{\tau_p}x\right) \tag{4}$$

$$B_n=\frac{1}{n}\sin\frac{n\pi\alpha_p}{2}\sinh\frac{n\pi h_m}{\tau_p} \tag{5}$$

$$\Lambda=\left(\sinh\frac{n\pi h_m}{\tau_p}+\mu_r\cosh\frac{n\pi h_m}{\tau_p}\right)e^{\frac{n\pi(L-h_m)}{\tau_p}}+\left(\sinh\frac{n\pi h_m}{\tau_p}-\mu_r\cosh\frac{n\pi h_m}{\tau_p}\right)e^{\frac{n\pi h_m}{\tau_p}} \tag{6}$$

2.3 Winding factor and EMF calculation

The back EMF can be solved according to the analytical formula of the air gap flux density. The end of the coreless concentrated winding is short in length and which ignore the end winding, as shown in Fig. 4(a). The w_c is coil side width, w_p is coil span. The coil number of the single concentrated winding is *N*. There are n_x turns in the *x* direction, and there are n_y turns in the *y* direction. That is $N=n_xn_y$. The electromotive force induced in each coil is expressed in Fourier series:

$$\frac{e(x)}{v_s}=\sum_{n=1,3,5...}^{\infty}E_n\sin\left(n\frac{\pi}{\tau_p}x\right) \tag{7}$$

where v_s is synchronous speed

$$E_n=2NLB_nk_w \tag{8}$$

N is the coil turns, *L* is the axial thickness of the motor. The winding factor k_w is determined by the pitch factor, the winding distribution factor in the *x* direction and the *y* direction distribution factor. The band factor distribution in the *x* direction can be seen from Fig. 4(c), which indicates the voltage reduction due to the width of the coil-band (w_c), can be calculated as:

$$\begin{aligned} k_{bn}&=n\frac{\int_0^{\frac{W_c}{2}}B_y\Delta r\Omega r\cos(\frac{x_i}{\tau_p}\pi)dx_i}{B_y\Delta r\Omega rW_c} \\ &=n\frac{2}{W_c}\int_0^{\frac{W_c}{2}}\cos(\frac{x_i}{\tau_p})dx_i \\ &=n\frac{2}{\pi}\frac{\tau_p}{W_c}\sin(\frac{\tau_p}{W_c}\frac{\pi}{2}) \end{aligned} \tag{9}$$

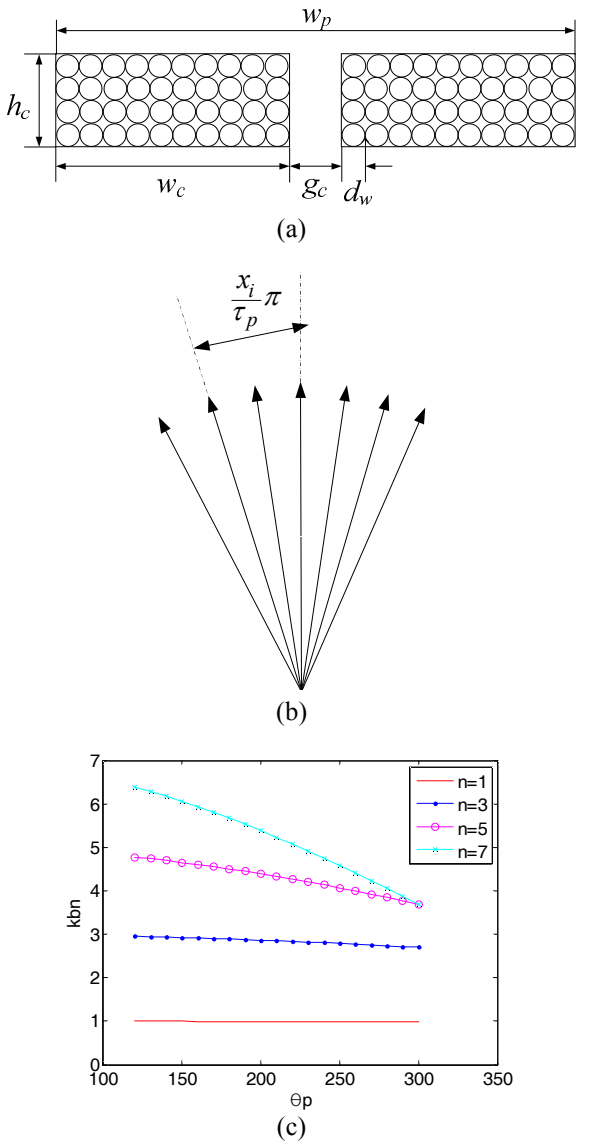

Fig. 4. Structure of coreless winding, (a) single concentrated winding, (b) single conductor EFM vector diagram, (c) band factor

When analyzing the induced back EMF in the coil, it is assumed that the conductor in the single side w_c region of the concentrated winding is uniformly distributed in the coil. The electromotive vector induced by all conductors in a single w_c region is shown in Fig. 4(b). The symmetrical center line is used as the reference line, and the back EMF of all the conductors are translated to the reference line. In the x_i distance reference line, the conversion factor of the conductor is $\cos \pi x_i / \tau_p$. When the fundamental wave is converted, the back EMF of each conductor is:

$$\Delta e_i(r) = B_y \Delta r \Omega r \cos(\frac{x_i}{\tau_p}\pi) \tag{10}$$

The back EMF of a single side coil with a wide conductor is:

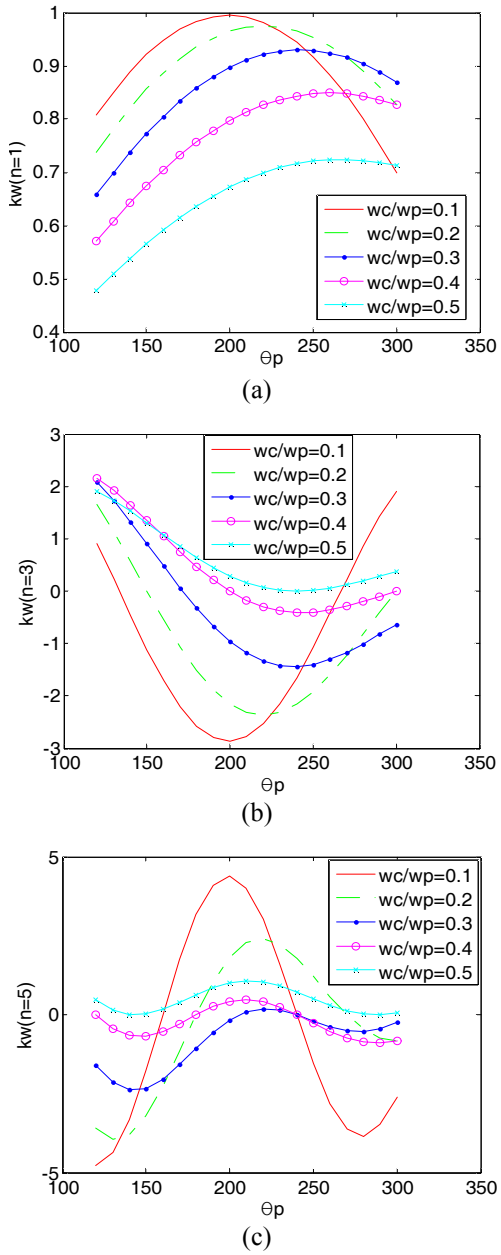

Fig. 5. Winding factor for different harmonics, (a) n=1, (b) n =3, (c) n =5, (d) n =7

$$\Delta e(r) = 2\int_0^{\frac{W_c}{2}} B_y \Delta r \Omega r \cos(\frac{x_i}{\tau_p}\pi) dx_i \tag{11}$$

The distribution factor of the width of the coil edge:

$$k_b = \frac{\int_0^{\frac{W_c}{2}} B_y \Delta r \Omega r \cos(\frac{x_i}{\tau_p}\pi) dx_i}{B_y \Delta r \Omega r W_c} = \frac{2}{W_c}\int_0^{\frac{W_c}{2}} \cos(\frac{x_i}{\tau_p}) dx_i = \frac{2}{\pi}\frac{\tau_p}{W_c}\sin(\frac{\tau_p}{W_c}\frac{\pi}{2}) \tag{12}$$

The coil span factor:

$$k_p = \sin\left(n\frac{\theta}{2} \right) = \sin\left(n\frac{W_p - W_c}{\tau_p}\frac{\pi}{2} \right) \quad (13)$$

The winding factor of n sub harmonic magnetic flux density:

$$k_w = k_b k_p = \frac{2\tau_p}{\pi W_c}\sin\left(n\frac{W_c}{\tau_p}\frac{\pi}{2} \right)\sin\left(n\frac{W_p - W_c}{\tau_p}\frac{\pi}{2} \right) \quad (14)$$

It can be seen from formula (14) that the winding factor is related to the coil span and the single width. The winding factor for fundamental component as well as third, fifth and seventh harmonic numbers are shown in Fig. 5 at different electrical angles and different w_c/w_p. The distribution rule provides a good basis for the generator to select the maximum fundamental amplitude and minimum harmonic content of the back EMF. As can be seen from Fig. 5, with the increasing ratio of the coil width w_c to the w_p, the fundamental harmonic factor of the winding and the seventh harmonic factor increase at first and then decrease. The third and fifth harmonic factor decreases at first and then increases. In order to obtain maximum fundamental wave and minimum harmonic content of the back EMF, the pitch of the windings should be selected at 200-250 angles and w_c/w_p is between 0.2-0.4.

2.4 Torque and efficiency calculation

A single-phase equivalent circuit of the coreless AFPMSG is depicted as shown in Fig. 6. Here, P_g and P_{FW} are generator input power and motor loss, respecttively. T_g and T_{FW} are the corresponding torque. The E_b, U_a, I_a, R_a and X_a are the back EMF, the terminal voltage, the phase current, the armature winding resistance and inductance of the generator, respectively. Among them, E_b, U_a, and I_a are valid values.

Without considering mechanical loss, the generator input power is given as:

$$P_g = T_g w_r = 3E_b I_a \quad (15)$$

The armature response of coreless stator axial flux permanent magnet synchronous generator is smaller, and it is difficult to generate significant eddy current losses in the rotor. The copper consumption of winding is larger than that of mechanical loss and eddy current loss, and the generator efficiency is given as:

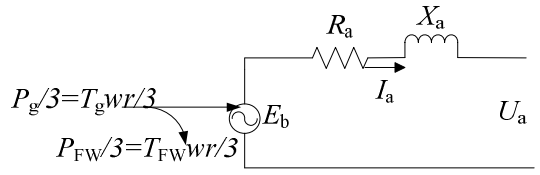

Fig. 6. Equivalent circuit for one phase of the AFPMSGa

$$\eta_g = \frac{3E_b I_a - P_{cu}}{3E_b I_a} \quad (16)$$

Fig. 6 shows that the generator mechanical energy is converted into electric energy. Since the coreless iron consumption is not considered, the instantaneous electromagnetic torque of the generator can be obtained from formula (17) :

$$T_g(t) = \left\{ e_a(t)i_a(t) + e_b(t)i_b(t) + e_c(t)i_c(t) \right\} / w_r \quad (17)$$

Where the subscript a, b, and c are the three phases, e is instantaneous back EMF and i is phase current.

3. Optimal Design

Industrial production has strict requirements for the sine wave of the electromotive force waveform of the synchronous generator. The deviation degree between the voltage waveform and the sine waveform is expressed by the voltage waveform distortion rate. which is given as:

$$THD = \frac{\sqrt{U_2^2 + U_3^2 + ... + U_n^2}}{U_1} \times 100\% \quad (18)$$

From the above knowledge, the harmonic content of back EMF is determined by the air gap flux density waveform and the winding width. It is a multi-objective and multivariable optimization process to obtain a back EMF with sinusoidal amplitude and high amplitude. The traditional single variable optimization method is time-consuming and difficult to find the optimal solution. In this paper, the formula (19) is used as the optimization objective, the pole arc coefficient a_p and the coil width w_c are taken as the optimization variables. The response surface method (RSM) is used to find the function relationship between the objective function and the variables.

$$\begin{cases} f_1 = \max \dfrac{\Delta e_1}{N} \\ f_2 = \min \dfrac{\sqrt{\sum_{n=3,5,.....}^{\infty} \Delta e(r)^2}}{\Delta e_1} \end{cases} \quad (19)$$

To construct the response surface and find the optimum conditions, an appropriate mathematical model is firstly established by the experimental data. The function relation between objective function and variable is usually established by using two order function:

$$y = \beta_0 + \beta_1 x_1 + \beta_2 x_2 + \beta_{11} x_1^2 + \beta_{22} x_2^2 + \beta_{12} x_1 x_2 + \varepsilon \quad (20)$$

Where y is the response objective function, β is the undetermined coefficient, ε is the fitting error, the x_1 and x_2

are the permanent magnet pole arc coefficient and the winding width coding value, respectively.

The fundamental magnitude and harmonic content of the back EMF are related to the pole arc factor a_p and the winding width w_c. Therefore, a mathematical model of the above two variables and the response objective can be established. The central composite surface design (CCF) method is used to fit the two response surface. After encoding, the low and high levels of independent variables and high school points were -1, 0, and +1, respectively.

Variable variation range:

$$\begin{aligned} 0.6 \le a_p \le 0.9 \\ 8 \le w_c \le 16 \end{aligned} \tag{21}$$

Total number of experimental designs:

$$n = 2^k + 2k + M \tag{22}$$

k is the number of variables, and M is the center point.

By optimizing the two factors of pole arc coefficient and coil edge width, the fundamental amplitude and harmonic content of back EMF are considered as the response values. Table 1 is the combination of design variables of the nine experimental points of formula (22):

According to the experimental data corresponding to the nine experimental schemes in Table 1, the optimal polar arc coefficient and the coil width can be solved by response surface methodology. A mathematical model for estimating amplitude of fundamental wave using least square method:

$$\begin{aligned} y = -35.8949 + 62.3159x_1 + 7.9982x_2 - \\ 42.4481x_1^2 - 0.3685x_2^2 + 0.3658x_1x_2 \end{aligned} \tag{23}$$

The mathematical model of THD for back EMF is given as:

$$\begin{aligned} y = 0.1353 - 0.7501x_1 + 0.0302x_2 + \\ 0.7453x_1^2 - 0.0085x_2^2 - 0.0218x_1x_2 \end{aligned} \tag{24}$$

where x_1, x_2 represent variable a_p, w_c, respectively.

Fig. 7 is the quantitative rule between the response target and the variable factor, which can solve the best combination of factors. The slope size of response surface

Table 1. CCF experimental design and results

Number	Variable		Coded conversion value		Fundamental amplitude/v	THD
	a_p	w_c	x_1	x_2		
1	0.6	8	-1	-1	28.4716	0.04243
2	0.9	8	+1	-1	28.7944	0.09518
3	0.6	16	-1	+1	23.4932	0.00648
4	0.9	16	+1	+1	24.6940	0.00694
5	0.6	12	-1	0	31.5395	0.03175
6	0.9	12	+1	0	32.7462	0.07423
7	0.75	8	0	-1	29.5128	0.04015
8	0.75	16	0	+1	24.8919	0.00497
9	0.75	12	0	0	32.3300	0.03308

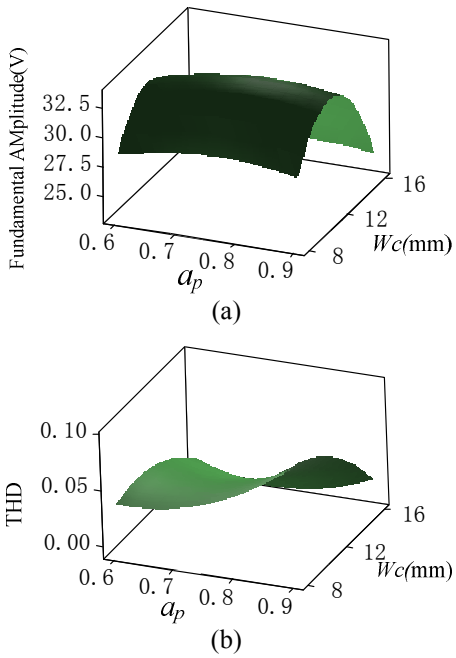

Fig. 7. RSM for polar arc and side width, (a) back EMF, (b) THD

reflects the significant influence of interaction between two variables on the response value. The steeper the slope is, the more significant the interaction effects on the response value. On the contrary, it is not significant. As shown in Fig. 7, when the polar arc coefficient is 0.7-0.9 and the width of the coil is between 12-16mm, the interaction between the two variables is significant to the fundamental amplitude and harmonic content of the back EMF. While when the polar arc coefficient is 0.6-0.7 and the width of the coil edge is between 8-12mm, the interaction between the two variables is not significant to the back EMF. By analyzing the contour map, we can get the optimal condition as (x_1, x_2)=(0.782, 15.241). According to the corresponding response, the fundamental amplitude of the back EMF is 27.8412 and THD is 0.0201. Taking into account the actual model of the generator and prototype production, taking a_p as 0.78 and w_c as 15mm, a finite element model is built to calculate the back EMF. The fundamental amplitude is 27.5137 and THD is 0.0248. The results of finite element analysis verify the validity of the multi-objective and multivariable response surface optimization method.

4. Model Verification and Experimental Test

According to the above analytic design method and the optimization results, a double external rotor and coreless internal stator permanent magnet generator is designed. The rated power of the prototype machine is 300W, the rated speed is 300r/min. The coreless stator is non overlapping concentrated windings. The main components of the prototype are shown in Fig. 8.

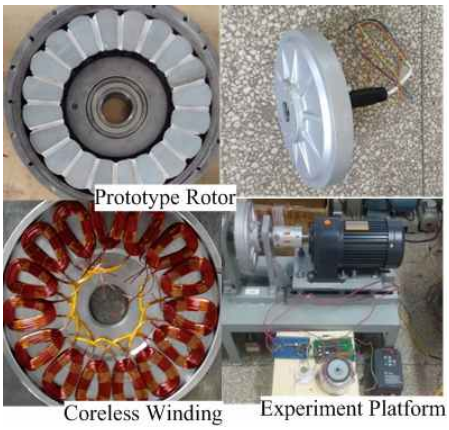

Fig. 8. Prototype machine and its main components

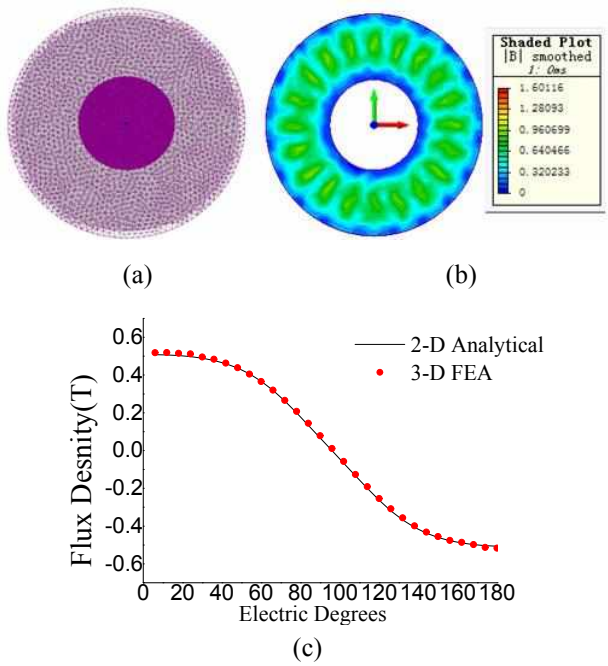

Fig. 9. (a) 3-D FEA mesh profiles, (b) flux density nephogram, (c) comparison of analytical results with 3-D FE results

In order to verify the validity of the 2-D magnetic field analytical model, 3-D finite element model of the prototype is established. Fig. 9(a) and Fig. 9(b) are 3-D finite element mesh profiles model and flux density nephogram of the prototype machine, respectively. As shown in the diagram, the maximum magnetic flux density is 1.6T, which is less than the maximum magnetic saturation value of rotor material 2.0T. There is no magnetic saturation in the parts of the motor. Comparisons the result of analytical method and finite element method in the air gap flux distribution along the circumferential gap are shown in Fig. 9 (c). The analytical method is in agreement with the finite element method. The calculated value of the analytic method is slightly smaller than that of the 3-D finite element simulation. The deviation occurs at the maximum position

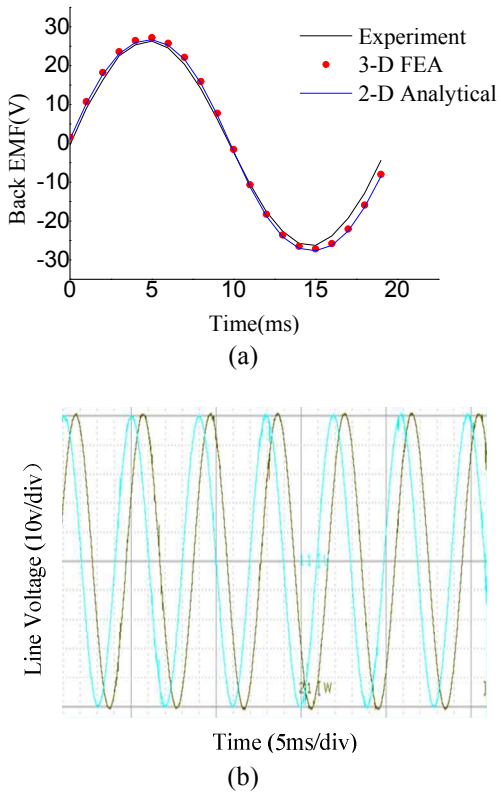

Fig. 10. No-load characteristic of generator, (a) comparison of three calculation methods, (b) measurements

of the axial magnetic flux density, but the error is less than 3%, which can fully meet the requirements of the preliminary design of the motor. The main reason for the deviation is that the analytical method does not consider the effects of magnetic saturation and magnetic flux leakage.

Using the prime mover to drag the generator to the rated speed. The measured phase voltage is compared with the 3-D finite element method and the analytical method as shown in Fig. 10(a) and the measured result of the prototype line voltage is shown in Fig. 10(b). As can be seen from Fig. 10(a), the waveforms calculated by the two methods are in good agreement with the measured waveforms. The maximum error is less than 7%, and the error is mainly caused by artificial machining. The 2-D analysis method is short in time and reduces the generator design time.

To verify the feasibility of 2-D analysis and response surface optimization method in this paper. Table 2 show the results of the three methods compared with the experimental. The results show that the maximum error of the back EMF is 6.93%, and the minimum error is 4.52% in response surface methodology. The calculation accuracy is higher, and the correctness of the analytic optimization method is also verified.

In order to verify the load carrying capacity of generator, the generator is connected with a three-phase symmetrical resistive load as shown in Fig. 11(a). When the load is constant, the output voltage increases with the speed. The

Table 2. Comparison results of different methods

Response value	2-D analytic	error	3-DFEA	error	RSM	error	Experiment
EMF	27.214	6.93%	27.5137	5.76%	27.8412	4.52%	29.1
THD	0.0216	5.36%	0.0248	5.96%	0.0201	5.02%	0.01001

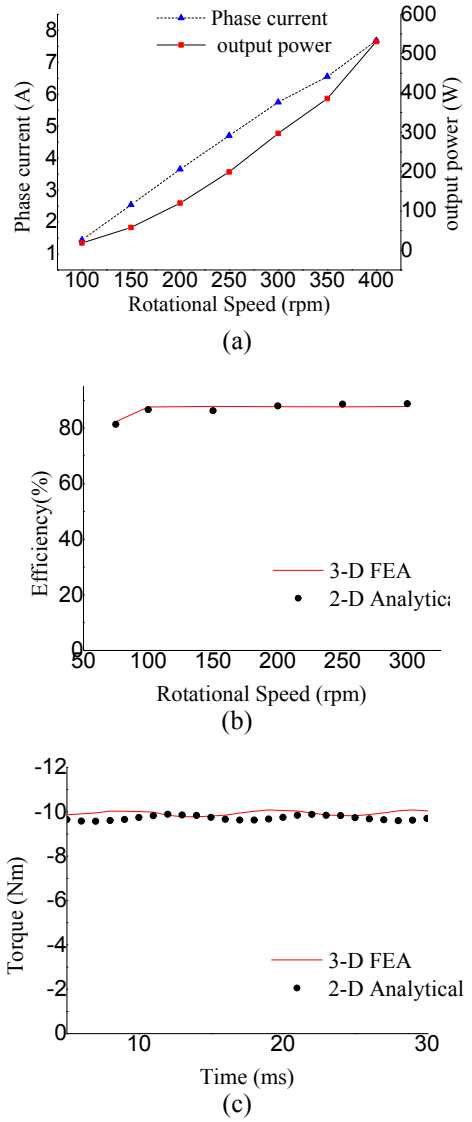

Fig. 11. Generator output characteristics under rated load, (a) output power and (b) efficiency under different speed, (c) torque at rated speed

current is directly proportional to the generator speed and the output power is directly proportional to the square of the current. When the speed is 300r/min, the output power is 297.39w, which meets the design requirements.

The generator electromagnetic torque (b) under rated load and the efficiency (c) under different speed are calculated by the finite element method and the analytic method, respectively. Which are shown in Fig. 11. Among them, efficiency calculation ignores mechanical loss, such as (14) and (15). The calculation results of the two methods are basically identical, and the validity and correctness of the 2-D analysis method are illustrated.

5. Conclusion

In this paper, the complexity of 3-D modeling and multi parameter optimization of axial magnetic field permanent magnet generator are discussed. A simple 2-D magnetic field analysis method and an analytical method for calculating the coreless concentrated winding factors of different structures are presented. This method is suitable for all kinds of coreless concentrated winding structure, which provides a good basis for selecting the maximum fundamental amplitude and the minimum harmonic content of the generator. The response surface methodology is applied to optimize the multi-objective and multivariable generators At last, a prototype is designed through this optimization method. The method is verified by 3-D finite element and experimental test. The results show that the parameters of the 2-D magnetic field analysis and coreless winding factor calculation method can accurately calculate the coreless stator axial flux permanent magnet generator, and the optimization method is short time consuming, which can find the optimal solution. This method can reduce the analysis time and calculation scale of the 3-D finite element model.

Acknowledgements

The study was supported by the key research project of science and technology of Henan Province (12A470004); key development and extension projects in Henan Province and the project supported by special funds for basic research and operation of colleges and universities of Henan Province(NSFRF140115); key research of development and promotion of Henan Provine (182102210052); mine power electronic device and control innovation type scientific and technological team of Henan Province.

References

[1] M. Chirca, S. Breban, C. Oprea and M. M. Radulescu, "Design Analysis of a Novel Double-Sided Axial-Flux Permanent-Magnet Generator for Micro-Wind Power Applications," *2014 International Conference on Optimization of Electrical and Electronic Equipment (OPTIM)*, Bran, pp. 472-476, 2014.

[2] Gieras J F, Wang R J, Kamper M. "Axial Flux

Permanent Magnet Brushless Machines," [M]. New Yoke: Springer Verlag, pp. 29-34, 2008.
[3] Min-Fu Hsieh and Yu-Sheng Hsu, "An Investigation on Influence of Magnet Arc Shaping Upon Back Electromotive Force Waveforms for Design of Permanent-Magnet Brushless Motors," in *IEEE Transactions on Magnetics*, vol. 41, no. 10, pp. 3949-3951, Oct. 2005.
[4] T. F. Chan and L. L. Lai, "An Axial-Flux Permanent-Magnet Synchronous Generator for a Direct-Coupled Wind-Turbine System," in *IEEE Transactions on Energy Conversion*, vol. 22, no. 1, pp. 86-94, March 2007.
[5] Rong-Jie Wang, M. J. Kamper, K. Van der Westhuizen and J. F. Gieras, "Optimal Design of a Coreless Stator Axial Flux Permanent-Magnet Generator," in *IEEE Transactions on Magnetics*, vol. 41, no. 1, pp. 55-64, Jan. 2005.
[6] J. Cros and P. Viarouge, "Synthesis of High Performance PM Motors With Concentrated Windings," in *IEEE Transactions on Energy Conversion*, vol. 17, no. 2, pp. 248-253, Jun 2002.
[7] M. J. Kamper, R. J. Wang and F. G. Rossouw, "Analysis and Performance of Axial Flux Permanent-Magnet Machine with Air-Cored Nonoverlapping Concentrated Stator Windings," in *IEEE Transactions on Industry Applications*, vol. 44, no. 5, pp. 1495-1504, Sept.-Oct. 2008.
[8] A. Hassanpour Isfahani, "Analytical Framework for Thrust Enhancement in Permanent-Magnet (PM) Linear Synchronous Motors With Segmented PM Poles," in *IEEE Transactions on Magnetics*, vol. 46, no. 4, pp. 1116-1122, April 2010.
[9] N. Roshandel Tavana and A. Shoulaie, "Analysis and Design of Magnetic Pole Shape in Linear Permanent-Magnet Machine," in *IEEE Transactions on Magnetics*, vol. 46, no. 4, pp. 1000-1006, April 2010.
[10] Song jianqiao. "Design and Research on Permanent Magnet Generator with Rotor and Fractional-Slot Concentrated Winding," [D] Harbin University of Science and Technology, 2013.
[11] Ren Yanping. "Design and Research on Permanent Magnet Generator with Circumferential Double-Layer and Fractional-slot Concentrated Winding," [D] Harbin University of Science and Technology, 2012.
[12] Xia Bing. "Study of Disc Type Permanent Magnet Machine for Small Vertical Axis Wind Power Application," [D]. Hangzhou: Zhejiang University, 2010.
[13] A. Mohammadpour, A. Gandhi and L. Parsa, "Winding Factor Calculation for Analysis of Back EMF Waveform in Air-Core Permanent Magnet Linear Synchronous Motors," in *IET Electric Power Applications*, vol. 6, no. 5, pp. 253-259, May 2012.
[14] R. J. Hill-Cottingham, P. C. Coles, J. F. Eastham, F. Profumo, A. Tenconi and G. Gianolio, "Multi-Disc Axial Flux Stratospheric Aircraft Propeller Drive," *Conference Record of the 2001 IEEE Industry Applications Conference. 36th IAS Annual Meeting (Cat. No.01CH37248)*, Chicago, IL, USA, pp. 1634-1639 vol.3, 2001.
[15] J. Y. Choi, S. H. Lee, K. J. Ko and S. M. Jang, "Improved Analytical Model for Electromagnetic Analysis of Axial Flux Machines With Double-Sided Permanent Magnet Rotor and Coreless Stator Windings," in *IEEE Transactions on Magnetics*, vol. 47, no. 10, pp. 2760-2763, Oct. 2011.
[16] Gyu-Hong Kang, Jung-Pyo Hong and Gyu-Tak Kim, "A Novel Design of an Air-core Type Permanent Magnet Linear Brushless Motor By Space Harmonics Field Analysis," in *IEEE Transactions on Magnetics*, vol. 37, no. 5, pp. 3732-3736, Sept. 2001.
[17] M. Aydin and M. Gulec, "A New Coreless Axial Flux Interior Permanent Magnet Synchronous Motor With Sinusoidal Rotor Segments," in *IEEE Transactions on Magnetics*, vol. 52, no. 7, pp. 1-4, July 2016.
[18] Wang Mingjie, Cheng Zhiping, Jiao Liucheng. "Analysis on the Sinusoidal Magnetic Field of Slotless PMLSM Using Modular Poles," [J]. *Electric Machines and Control*, vol. 19, no. 4, pp. 34-39, 2015.
[19] Y. Shen and Z. Q. Zhu, "Investigation of Permanent Magnet Brushless Machines Having Unequal-Magnet Height Pole," in *IEEE Transactions on Magnetics*, vol. 48, no. 12, pp. 4815-4830, Dec. 2012.
[20] M. Markovic and Y. Perriard, "Optimization Design of a Segmented Halbach Permanent-Magnet Motor Using an Analytical Model," in *IEEE Transactions on Magnetics*, vol. 45, no. 7, pp. 2955-2960, July 2009.

Zhujun He received his PH.D degree in college of Mechanical and Electrical Engineering, Inner Mongolia Agricultural University, China, in 2010. Currently, He is an Assistant Professor in School of Electrical Engineering and Automation, Henan Polytechnic University, China. His research interests are wind power generation, special motor design and drive.

Li Shaolong He received his bachelor's degree in college of Electrical Engineering and Automation, Luoyang Institute of Science and Technology, China, in 2015. Currently, He is a master's graduate student in the School of Electrical Engineering and Automation, Henan Polytechnic University, China. His research interests are wind power generation and design of permanent magnet motor

Song dandan She received his bachelor's degree in college of Wanfang science and Technology College of Henan Polytechnic University, China, in 2016. Currently, she is a master's graduate student in the School of Electrical Engineering and Automation, Henan Polytechnic University, China. Her major research is magnetic levitation wind power generation.

Han Qiaoli She received her PH.D degree in college of Mechanical and Electrical Engineering, Inner Mongolia Agricultural University, China, in 2006. Currently, she is an Associate Professor in College of Energy and Transport-ation Engineering, Inner Mongolia Agricultural University, China. Her major research interest is wind power technology.

Li Guanghua He received his bachelor's degree in college of Electri-cal Engineering and Automation, Pingdingshan University, China, in 2017. Currently, He is a master's graduate student in the School of Electrical Engineering and Automation, Henan Polytechnic University, China. His research interests are wind power generation and design of permanent magnet motor.